Supplementary Figure 1

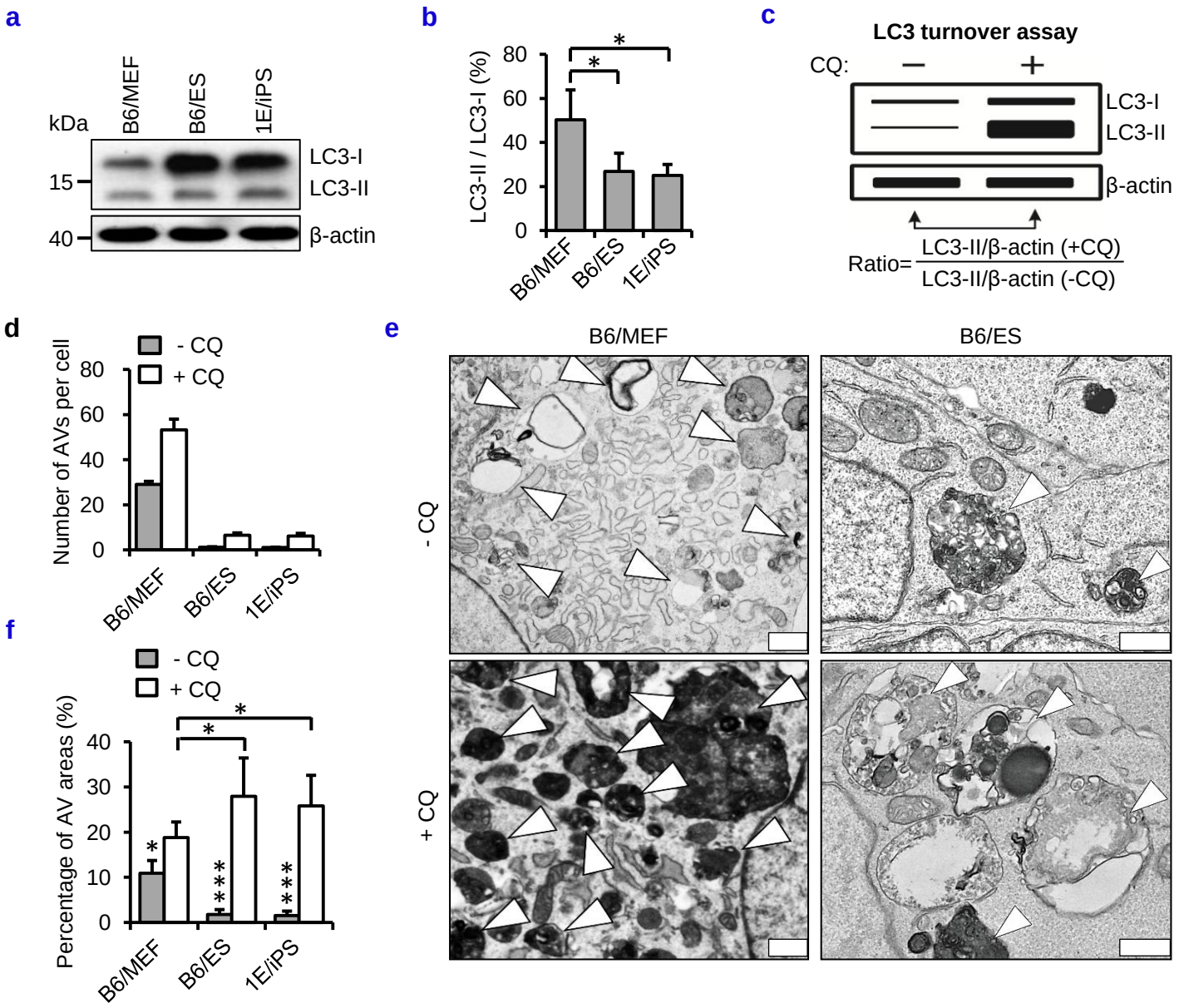

Supplementary Figure 1 High autophagic flux in PSCs. a, LC3 differences between B6/MEF, B6/ES and 1E/iPS cells. β-actin served as the loading control. **b**, Quantification of the percentage of the conversion of LC3-I (cytosolic form) to LC3-II (lipidated form) in a. Data shown are mean ± s.d., n=4, *P<0.05 (Student's *t*-test). **c**, Schematic of the method to monitor autophagic flux using LC3 turnover assay. Autophagic flux was measured according to the difference of LC3-II levels between untreated and lysosomal inhibitor treated samples. **d**, Statistical analysis of the number of autophagic vacuoles (AVs) per cell with or without CQ treatment in Figure 1c. Data shown are mean ± s.d., n=20. **e**, Magnified TEM pictures of B6/MEF and B6/ES with or without CQ-treatment. scale bars, 1 μm. **f**, Quantification of the percentage of AV areas in randomly sampled cell from Figure 1c. Data shown are mean ± s.d., n=8, *P<0.05, ***P<0.001 (Student's *t*-test). Image in a is representative of 3 independent experiments.

Supplementary Figure 2

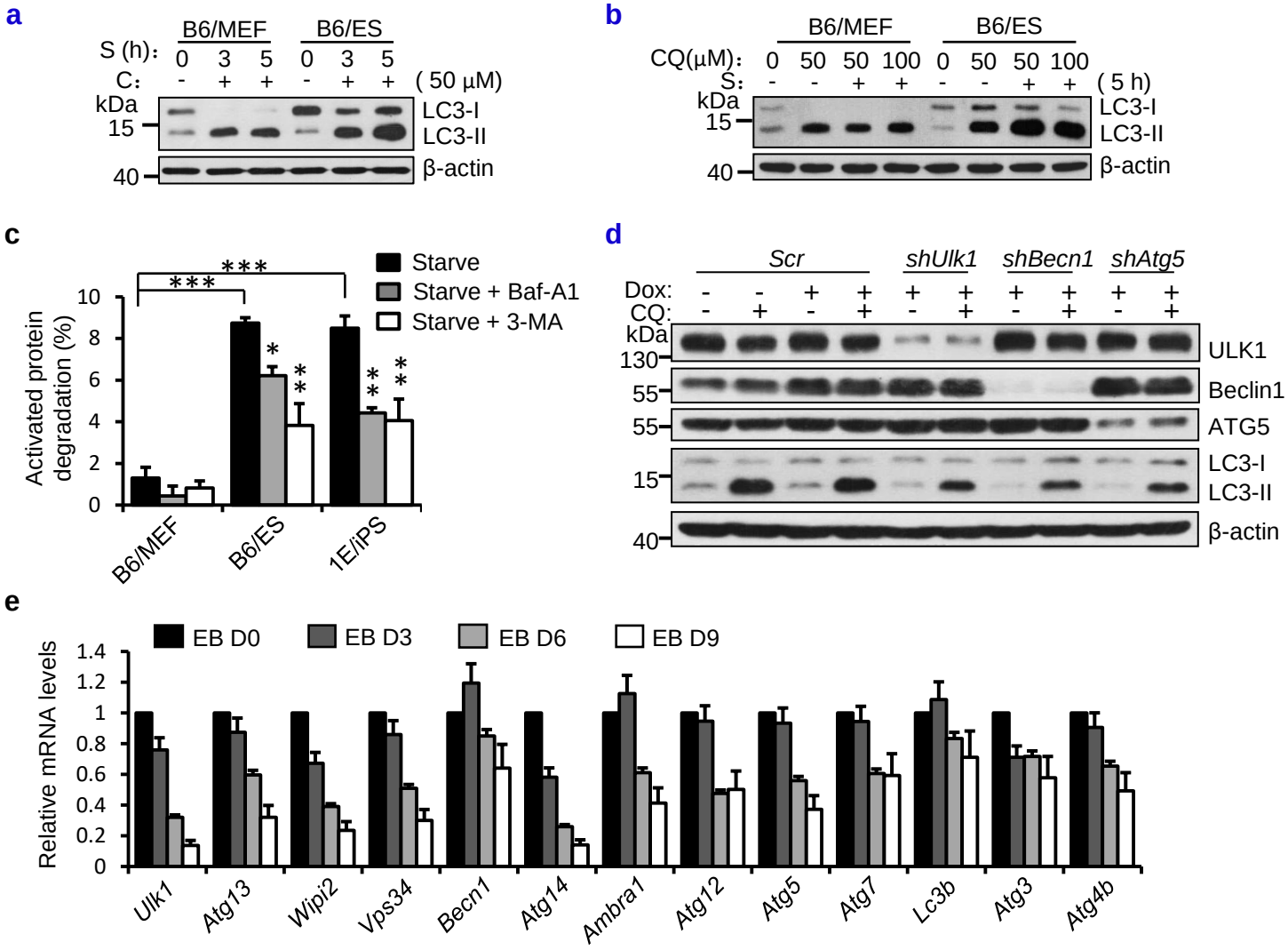

Supplementary Figure 2 PSCs have a high autophagic potency in response to stress. a, Western blotting for LC3 in B6/MEF and B6/ES cells under starvation conditions. Cells underwent EBSS starvation for 3 or 5 h. CQ treatment: 50 μM. β-actin served as the loading control. **b**, Western blotting for LC3 in B6/MEF and B6/ES cells under starvation conditions and different dose concentration of CQ. Cells underwent EBSS starvation for 5 h. CQ treatment: 50 or 100 μM. β-actin served as the loading control. **c,** Long-lived protein degradation in B6/MEF, B6/ES, and 1E/iPS cells under EBSS starvation conditions (5 h). Inhibition of degradation of long-lived proteins induced by bafilomycin A1 (Baf-A1, 20 nM) or 3-MA (10 mM). Data shown are mean ± s.d., n=3, *P<0.05, **P<0.01, ***P<0.001 (Student's *t*-test). **d,** qPCR for autophagy-related genes during ESC differentiation. **e,** Western blotting for ULK1, Beclin1, ATG5 and LC3 in Dox-induce KD ESC lines. β-actin served as the loading control. Dox, Doxycycline. Dox treatment: 100 ng/ml, 72 h. Images in a, b and d are representative of 3 independent experiments respectively.

Supplementary Figure 3

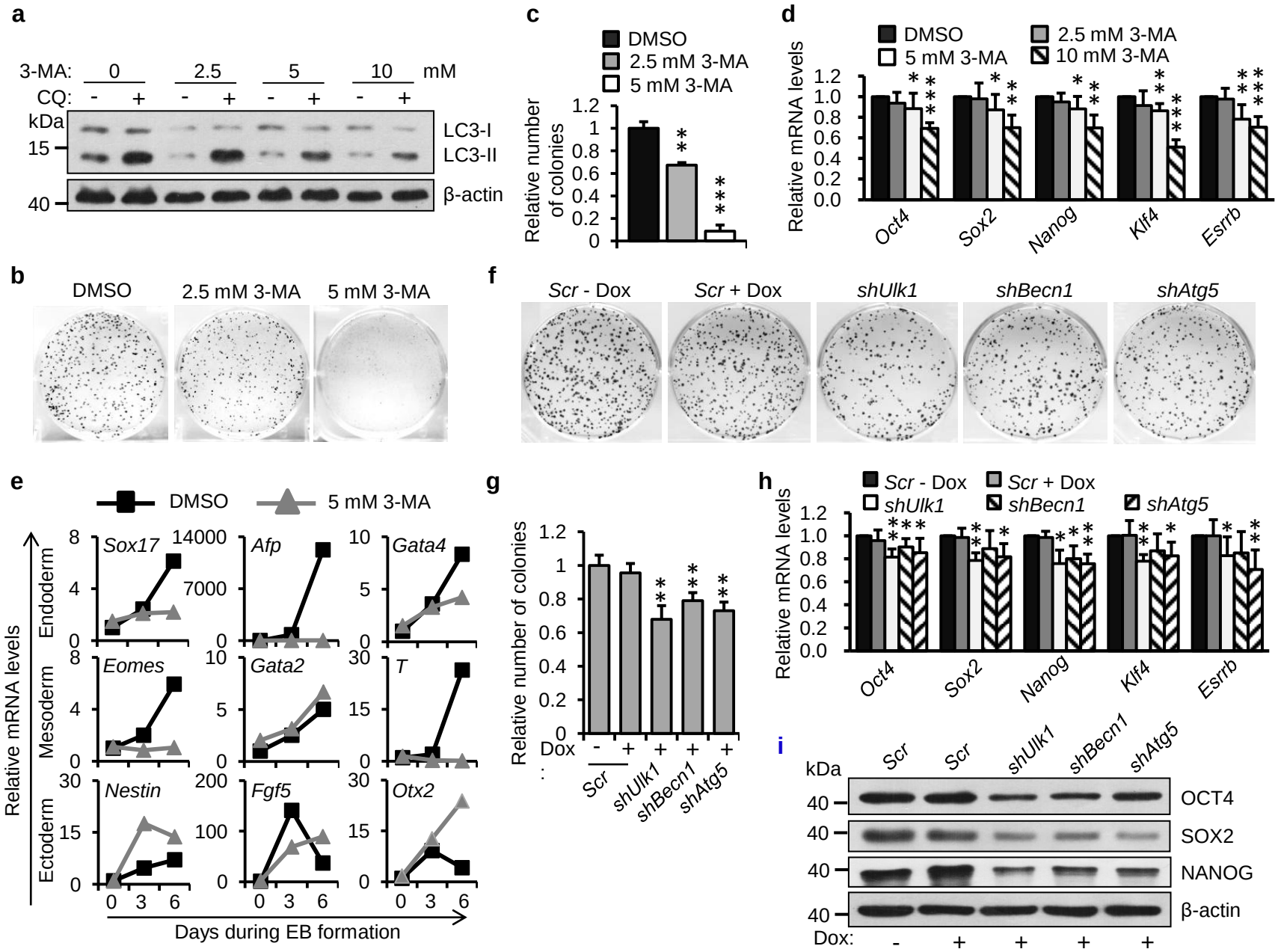

Supplementary Figure 3 Autophagy inhibition by 3-MA or autophagy gene silencing disrupts ESC identity. **a,** Western blotting for LC3 in B6/ES cells treated with indicated amount of 3-MA for 12 h. β-actin served as the loading control. **b**, Representative images of colony formation by B6/ES cells treated with 3-MA for 7 days. **c**, Quantification of AP positive colonies in b. Data shown are mean ± s.d., n=3, **P<0.01, ***P<0.001 (Student's *t*-test). **d**, qPCR for pluripotency marker genes in B6/ES cells treated with 3-MA 12 h. Data shown are mean ± s.d., n=3, *P<0.05, **P<0.01, ***P<0.001 (Student's *t*-test). **e**, qPCR for lineage-specific marker genes during B6/ESC EB differentiation with or without 3-MA treatment. **f**, Representative images of colony formation by KD ESCs induced with Dox (100 ng/ml, 7 d). **g**, Quantification of AP positive colonies in f. Data shown are mean ± s.d., n=3, **P<0.01 (Student's *t*-test). **h,** qPCR for pluripotency marker genes in Dox-induced (100 ng/ml, 72 h) KD ESC lines. Data shown are mean ± s.d., n=3, *P<0.05, **P<0.01 (Student's *t*-test). i, Western blotting for OCT4, SOX2, and NANOG in Dox-induced (100 ng/ml, 72 h) KD ESC lines. β-actin served as the loading control. Images in a and i are representative of 3 independent experiments respectively.

Supplementary Figure 4

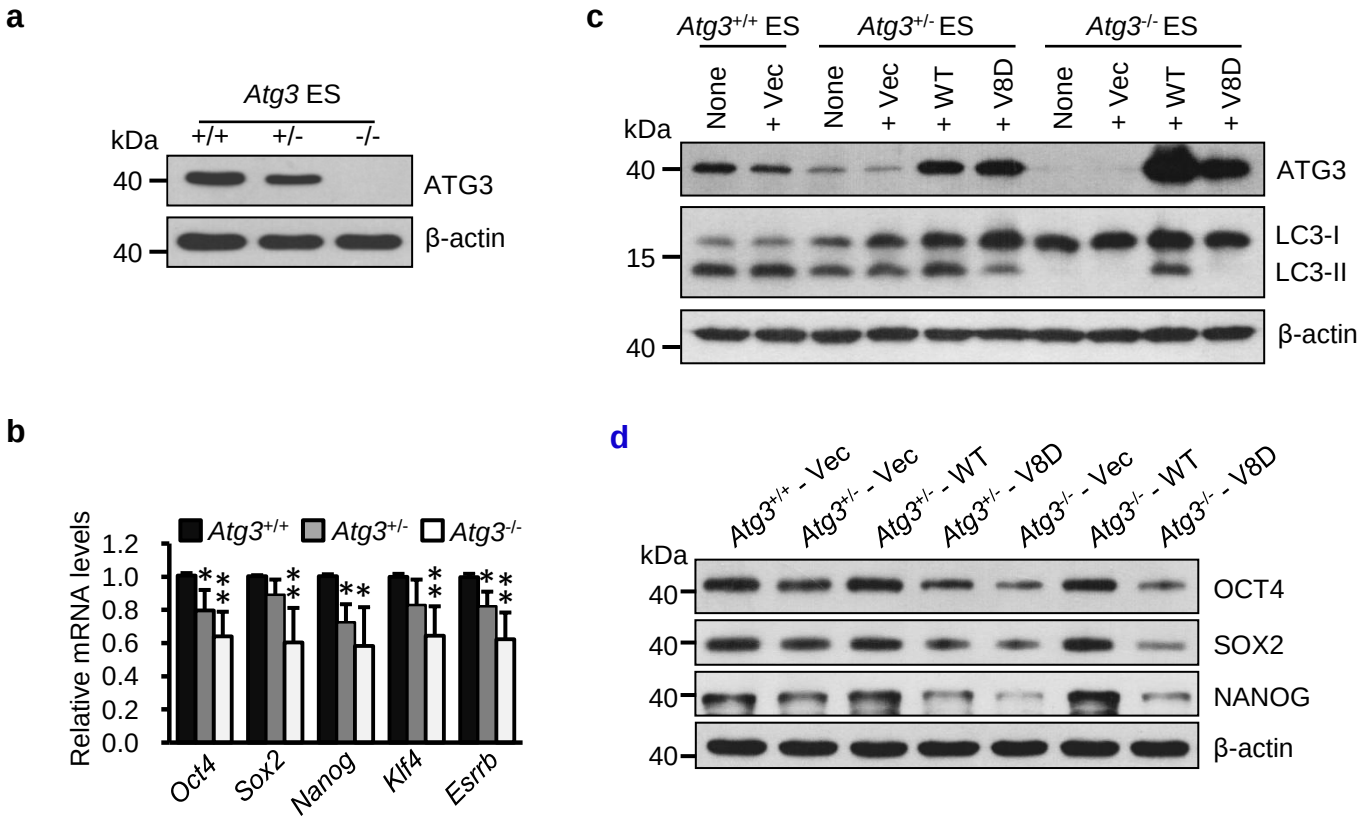

Supplementary Figure 4 Tapering autophagic flux compromises ESC pluripotency. a, Western blotting for ATG3 in *Atg3*$^{+/+}$, *Atg3*$^{+/-}$, and *Atg3*$^{-/-}$ ESCs. β-actin served as the loading control. **b**, Western blotting for ATG3 and LC3 in ATG3 rescue ESC lines. β-actin served as the loading control. All samples were treated with CQ (50 μM) for 5 h. **c,** qPCR for pluripotency marker genes in *Atg3*$^{+/+}$, *Atg3*$^{+/-}$, and *Atg3*$^{-/-}$ ESCs. Data shown are mean ± s.d., n=3, *P<0.05, **P<0.01 (Student's *t*-test). d, Western blotting for OCT4, SOX2, and NANOG in ATG3 rescue ESC lines. β-actin served as the loading control. Images in a, b and d are representative of 3 independent experiments respectively.

Supplementary Figure 5

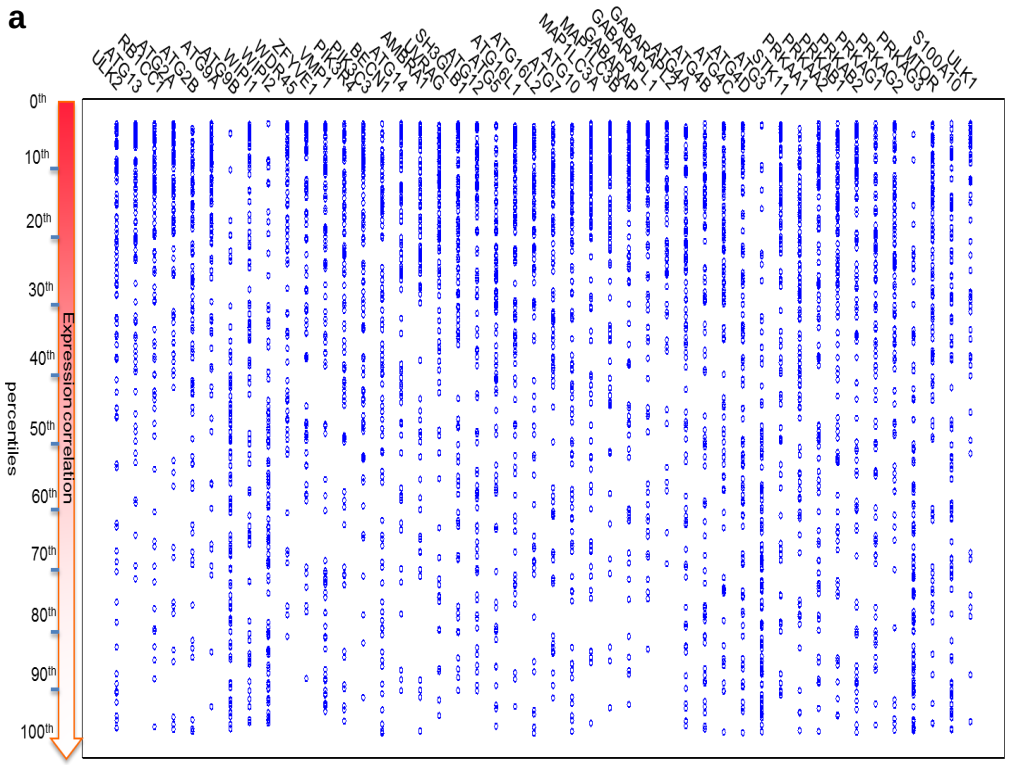

Supplementary Figure 5 Autophagy-related genes harbor FOXO binding motifs. a, Autophagy-related genes exhibit coordinated expression behavior. The diagram shows a representation of expression correlations among autophagy core machinery genes. Each column represents the ~22,690 gene probes of the Affymetrix MOE430A_2.0 platform ranked by expression correlation with the relevant gene indicated at the top. Blue bars represent the position of autophagy genes within the ranked lists. There was an enrichment of autophagy-related genes within the first 20th percentile of ranked lists of expression correlations. **b,** Bioinformatic analysis predicts FOXO binding motifs. **c,** Statistical analysis of FOXO binding motifs within regulatory regions of autophagy related genes. **d**, FOXO1 binding motifs investigated by ChIP analysis. **e**, Western blotting for FOXO1 during EB differentiation. β-actin served as the loading control. Image in e is representative of 3 independent experiments.

Supplementary Figure 6

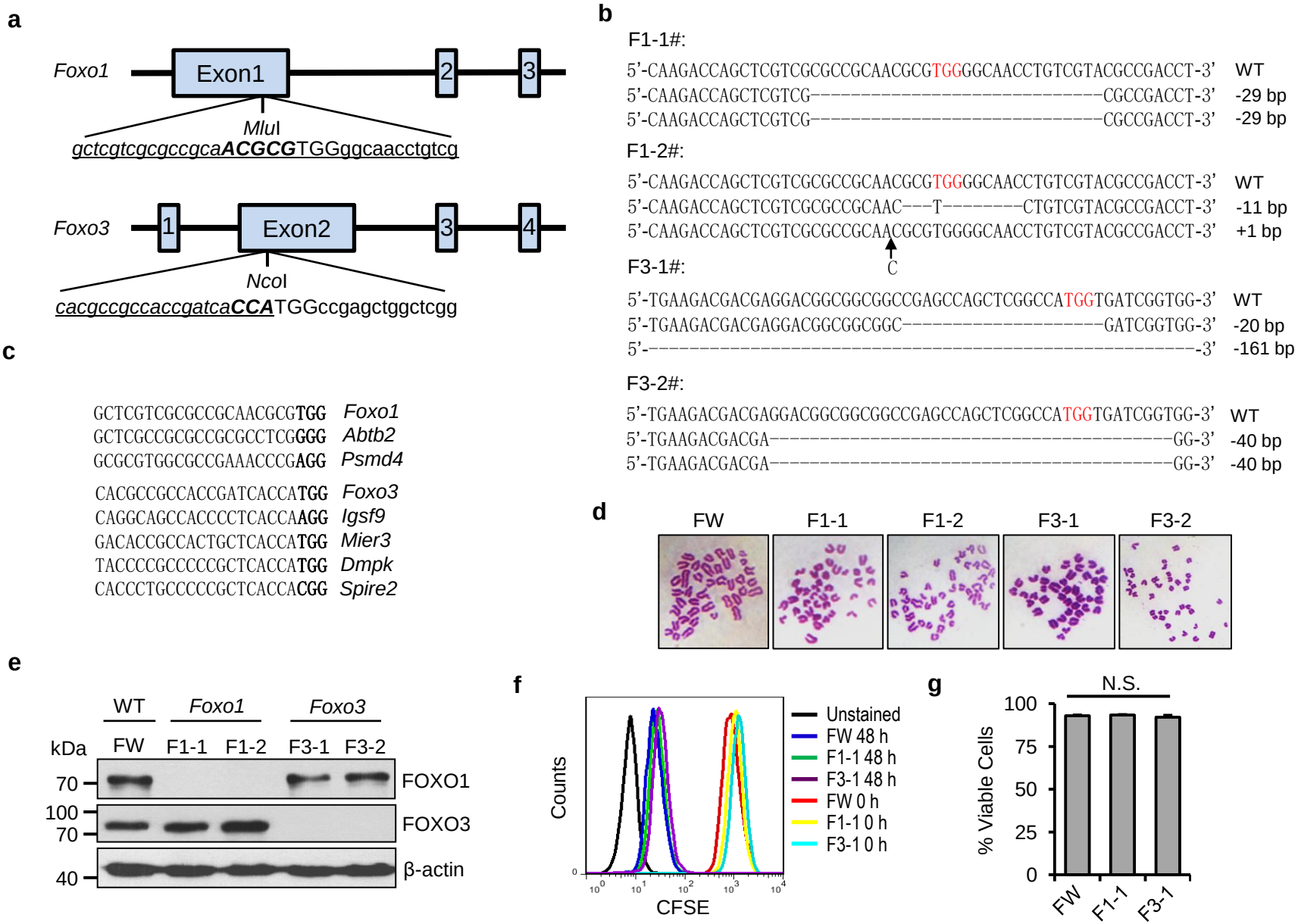

Supplementary Figure 6 Generation of *Foxo1* and *Foxo3* knockout ESCs by CRISPR-Cas9. a, Schematic of Cas9/sgRNA-targeting sites in *Foxo1* and *Foxo3.* The sgRNA-targeting sequence is underlined, and the protospacer-adjacent motif (PAM) sequence is capitalized. The restriction sites at the target regions are in italic, bold, and capitalized text. The restriction enzymes *Mlu*I and *Nco*I used for RFLP analysis are shown. **b,** Sequence analysis of *Foxo1*$^{-/-}$ and *Foxo3*$^{-/-}$ ESC lines. The PAM sequence is labeled in red. **c**, Off-target analysis of *Foxo1*$^{-/-}$ and *Foxo3*$^{-/-}$ ESC lines. Off-target sites were not found in potential off-target loci. **d,** Karyotype of *Foxo1*$^{-/-}$ and *Foxo3*$^{-/-}$ ESC lines. Chromosome number = 40. **e,** Western blotting for FOXO1 and FOXO3 in *Foxo1*$^{-/-}$ and *Foxo3*$^{-/-}$ ESC lines respectively. β-actin served as the loading control. **f,** Proliferation detection for *Foxo1*$^{-/-}$ and *Foxo3*$^{-/-}$ ESC lines. Carboxyfluorescein succinimdyl ester (CFSE)-labeled ESCs were analyzed by flow cytometry at 0 and 48 h. **g**, Apoptosis detection in *Foxo1*$^{-/-}$ and *Foxo3*$^{-/-}$ ESC lines. Cells that were double negative for PI and annexin-V were referred to as viable cells. Data shown are mean ± s.d., n=3; N.S., no significance (Student's t-test). Image in e is representative of 3 independent experiments.

Supplementary Figure 7

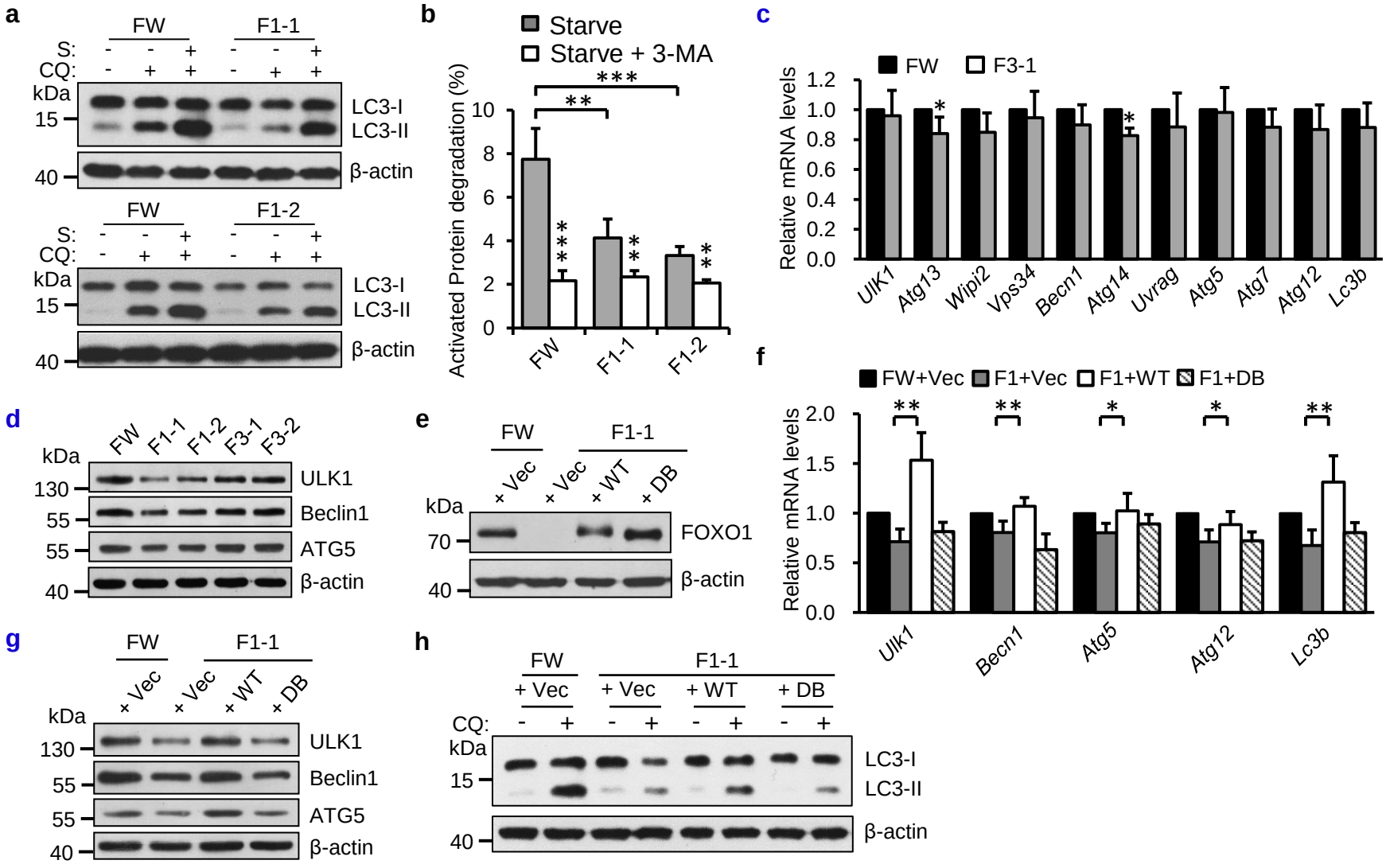

Supplementary Figure 7 FOXO1 regulates autophagic flux. a, Western blotting for LC3 in *Foxo1*$^{-/-}$ ESC lines. β-actin served as the loading control. **b,** Degradation of long-lived proteins in *Foxo1*$^{-/-}$ ESC lines under EBSS starvation conditions (5 h) with or without 3-MA treatment (10 mM, 5 h). Data shown are mean ± s.d., n=3, **P<0.01, ***P<0.001 (Student's *t*-test). **c**, qPCR for autophagy-related genes in *Foxo3*$^{-/-}$ ESC lines. Data shown are mean ± s.d., n=3, *P<0.05 (Student's *t*-test). **d**, Western blotting for ULK1, Beclin1, and ATG5 in *Foxo1*$^{-/-}$ and *Foxo3*$^{-/-}$ ESC lines. β-actin served as the loading control. **e**, Western blotting for FOXO1 in FOXO1 rescue ESC lines. β-actin served as the loading control. **f**, qPCR for autophagy-related genes in FOXO1 rescue ESC lines. Data shown are mean ± s.d., n=3, *P<0.05, **P<0.01 (Student's *t*-test). **g**, Western blotting for ULK1, Beclin1, and ATG5 in FOXO1 rescue ESC lines. β-actin served as the loading control. **h**, Western blotting for LC3 in FOXO1 rescue ESC lines. β-actin served as the loading control. Images in a, d, e, g, and h are representative of 3 independent experiments respectively.

Supplementary Figure 8

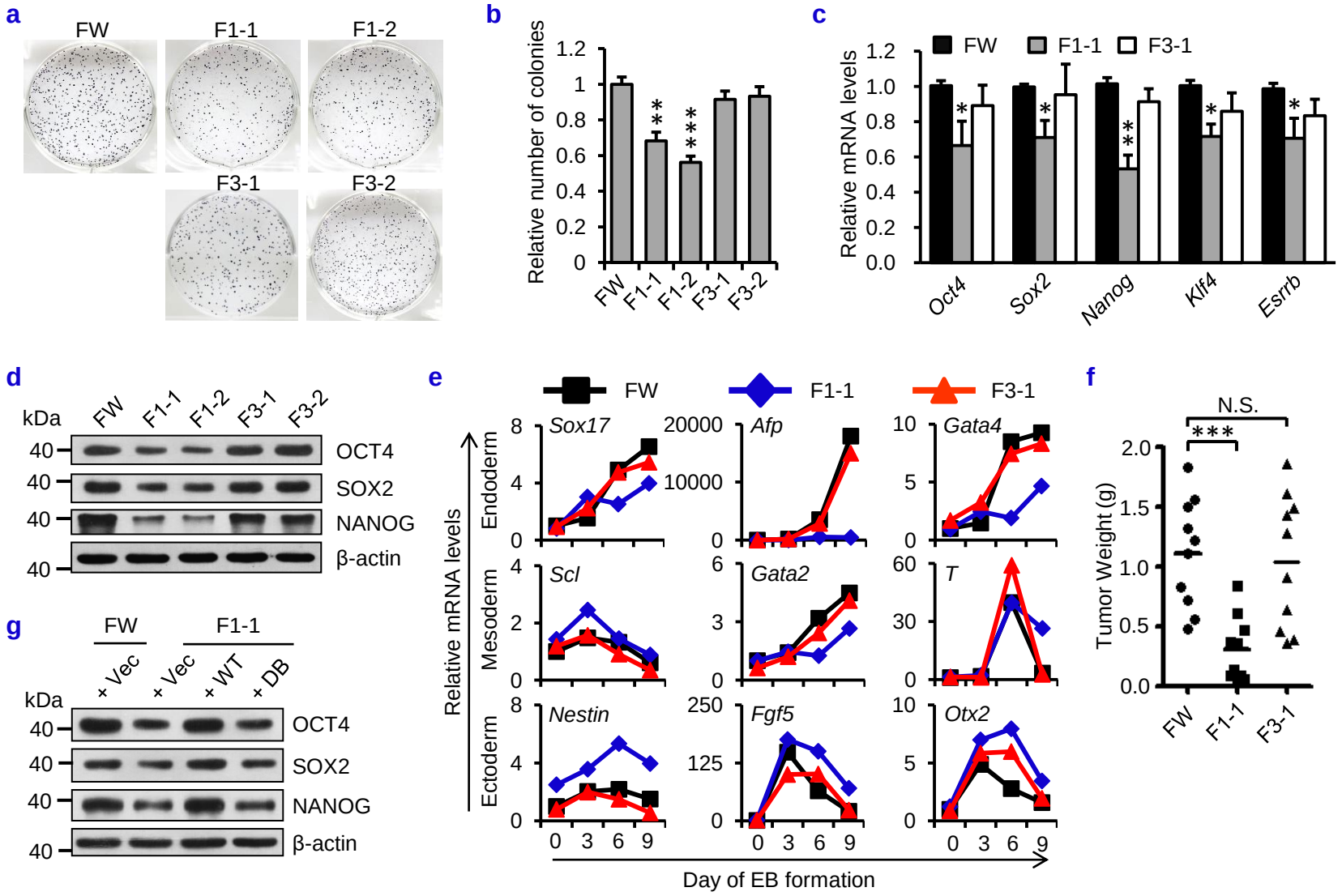

Supplementary Figure 8 *Foxo1* deletion impairs ESC self-renewal and differentiation. **a**, Representative images of colony formation by *Foxo1*$^{-/-}$ and *Foxo3*$^{-/-}$ ESC lines. **b**, Quantification of AP positive colonies in a. Data shown are mean ± s.d., n=3, **P<0.01, ***P<0.001 (Student's *t*-test). **c,** qPCR for pluripotency marker genes in *Foxo1*$^{-/-}$ and *Foxo3*$^{-/-}$ ESCs. Data shown are mean ± s.d., n=3, *P<0.05, **P<0.01 (Student's *t*-test). **d**, Western blotting for OCT4, SOX2, and NANOG in *Foxo1*$^{-/-}$ and *Foxo3*$^{-/-}$ ESCs. β-actin served as the loading control. **e**, qPCR for lineage-specific markers during *Foxo1*$^{-/-}$ and *Foxo3*$^{-/-}$ ESC EB differentiation in vitro. **f**, Statistical analysis of the weight of teratomas formed by *Foxo1*$^{-/-}$ and *Foxo3*$^{-/-}$ ESC lines; ***P<0.001, N.S., no significance (Student's *t*-test). **g**, Western blotting for OCT4, SOX2, and NANOG in FOXO1 rescue ESCs. β-actin served as the loading control. Images in d and g are representative of 3 independent experiments respectively.